CONDENSED MATTER PHYSICS

Engineered spin-orbit interactions in $LaAlO_3/SrTiO_3$-based 1D serpentine electron waveguides

Megan Briggeman[1,2], Jianan Li[1,2], Mengchen Huang[1,2], Hyungwoo Lee[3], Jung-Woo Lee[3], Kitae Eom[3], Chang-Beom Eom[3], Patrick Irvin[1,2], Jeremy Levy[1,2]*

The quest to understand, design, and synthesize new forms of quantum matter guides much of contemporary research in condensed matter physics. One-dimensional (1D) electronic systems form the basis for some of the most interesting and exotic phases of quantum matter. Here, we describe a family of quasi-1D nanostructures, based on $LaAlO_3/SrTiO_3$ electron waveguides, in which a sinusoidal transverse spatial modulation is imposed. These devices display unique dispersive features in the subband spectra, namely, a sizeable shift (~7 T) in the spin-dependent subband minima, and fractional conductance plateaus. The first property can be understood as an engineered spin-orbit interaction associated with the periodic acceleration of electrons as they undulate through the nanowire (ballistically), while the second property signifies the presence of enhanced electron-electron scattering in this system. The ability to engineer these interactions in quantum wires contributes to the tool set of a 1D solid-state quantum simulation platform.

INTRODUCTION

Some of the most celebrated electronic states of matter (e.g., integer and fractional Hall effect, quantum spin Hall states) can be described by one-dimensional (1D) models (*1*). In one dimension, the Fermi liquid description breaks down, and transport can be described by Tomononga-Luttinger models governing various collective modes that exhibit spin-charge separation, fractional charges, and non-Abelian statistics.

One approach to the grand challenge of understanding quantum matter is through "quantum simulation"—the creation of a highly configurable many-body quantum system is developed in which its Hamiltonian description can be related to relevant physical models (*2*–*4*). Quantum simulation necessarily requires a physical platform that can be configured to match or approximate the system of interest. Among the many quantum systems being developed for this purpose, ultracold atoms trapped within standing waves of light (*5*) have been particularly successful, in large part because the model Hamiltonians are well characterized and based on a fundamental understanding of the constituent atomic systems. For example, hyperfine states of trapped ions have been greatly successful in simulating classes of spin chains (*6*, *7*). Superconducting networks can also be used to simulate a wide range of Hamiltonians (*8*), while atom-scale manipulation [e.g., donor atoms in silicon (*9*) or arrangements of CO molecules (*10*)] has successfully emulated band structure and topological phases.

The type of quantum systems that can be explored in a quantum simulator is often limited by the available interactions of the host material. To increase the available physical interactions, a variety of pseudomagnetic fields (*11*, *12*), gauge fields (*13*), and spin-orbit interactions (*14*) can be added. Interparticle interactions can be controlled in a variety of ways, e.g., via Feshbach resonance in atomic systems or by coupling to a polarizable medium (*15*).

The complex-oxide $SrTiO_3$ has a wide range of gate-tunable properties that include superconductivity, magnetism, ferroelectricity, and ferroelasticity (*16*). Using a conductive atomic force microscopy (c-AFM) lithography technique, the $LaAlO_3/SrTiO_3$ interfacial conductivity (and related properties) can be programmed with a precision of 2 nm (*17*, *18*), comparable to the mean separation between electrons. The combination of a rich palette of intrinsic properties and the ability to form complex nanostructures provides a suitable foundation for the creation of a 1D quantum simulation platform.

A useful starting point for developing programmable 1D quantum systems is the $LaAlO_3/SrTiO_3$ electron waveguide (*19*). These devices exhibit highly quantized ballistic transport, in which the conductance is quantized in units of e^2/h, where e is the electron charge and h is the Planck constant. Each of the N occupied 1D subbands (arising due to vertical, lateral, and spin degrees of freedom) contributes one quantum of conductance to the total conductance $G = Ne^2/h$. A variety of correlated electronic phases have been identified, including a paired liquid phase (*19*, *20*), reentrant pairing (*19*), and a family of emergent composite electron liquids composed of bound states formed from 2, 3, 4, … electrons (*21*). The calculated wave functions of a representative electron waveguide device are shown in Fig. 1B, where the state $|m, n, s\rangle$ is identified by its quantum numbers m, n, and s that characterize the transverse orbital and spin degrees of freedom. Much of the unusual transport characteristics come from interactions between these various electronic subbands.

One property that appears to be lacking (or weak) in $LaAlO_3/SrTiO_3$ electron waveguides is spin-orbit coupling. Gate-tunable spin-orbit coupling has been reported at the 2D $LaAlO_3/SrTiO_3$ interface (*22*, *23*); however, detailed modeling of the subband spectra has ruled out such interactions for the most part in 1D quantum wires (*19*). Strong spin-orbit interactions are believed to be the "missing ingredient" in efforts to create Majorana zero modes (*24*, *25*) in these 1D quantum wires. A reasonable goal is therefore to engineer spin-orbit interactions in quantum wires, using the nanoscale control enabled by c-AFM lithography.

Here, we present transport experiments on ballistic electron waveguides that are perturbed by a periodic transverse ("serpentine")

[1]Department of Physics and Astronomy, University of Pittsburgh, Pittsburgh, PA 15260, USA. [2]Pittsburgh Quantum Institute, Pittsburgh, PA 15260, USA. [3]Department of Materials Science and Engineering, University of Wisconsin-Madison, Madison, WI 53706, USA.
*Corresponding author. Email: jlevy@pitt.edu

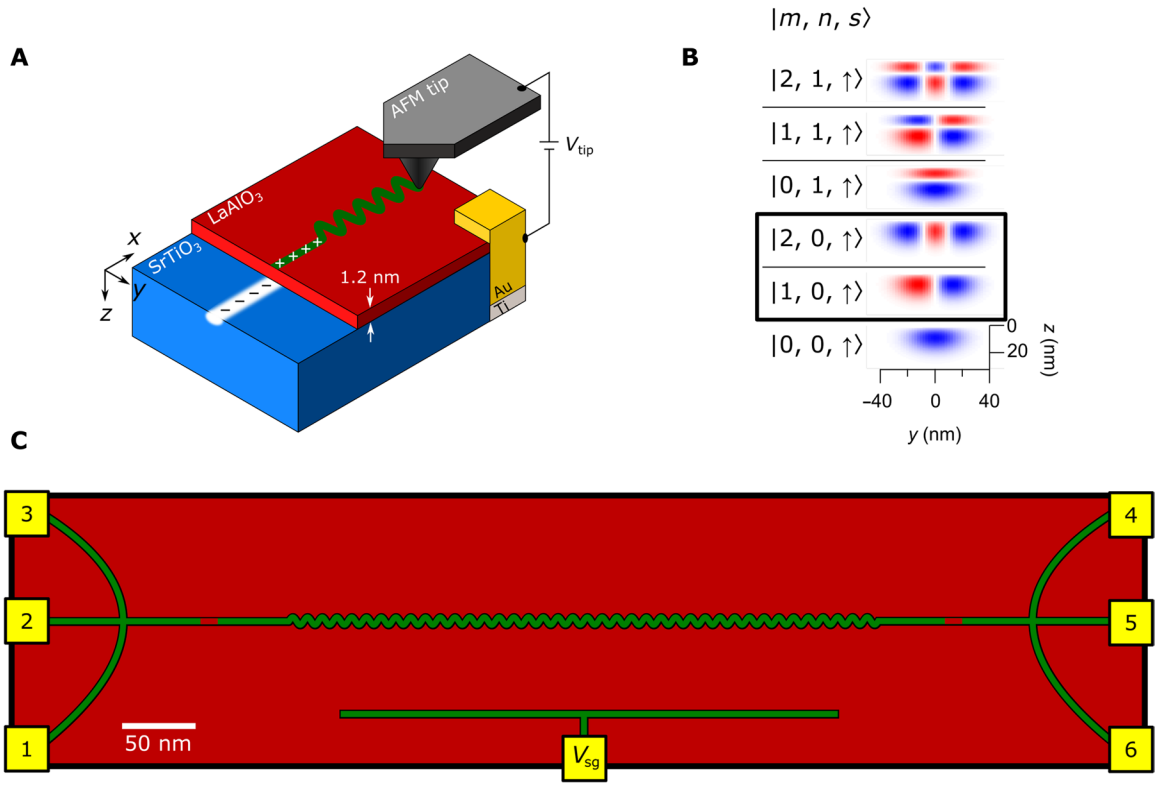

Fig. 1. Conductive AFM writing and device schematic. (**A**) Nanowires created at the $LaAlO_3/SrTiO_3$ interface using c-AFM lithography. A positive bias applied to the AFM tip protonates the surface, causing electrons to accumulate at the interface. One-dimensional serpentine superlattice devices are created by laterally modulating the tip position on the $LaAlO_3$ surface. (**B**) Representative wave functions calculated for an electron waveguide device with vertical, lateral, and spin degrees of freedom (*19*). The serpentine motion of the superlattice couples the ground state of the waveguide with different lateral modes of the waveguide (modes circled in black). (**C**) Schematic for the 1D serpentine superlattice devices. c-AFM written paths (green lines) represent the device and are connected to interface electrodes (yellow). The serpentine lateral modulation is bracketed by highly transparent tunnel barriers similar to those used to create electron waveguide devices (*19*). The voltage/current leads are used to take a four-terminal measurement of the device. A local side gate is also created using c-AFM lithography. A voltage applied to the gate (V_{sg}) changes the chemical potential of the the device.

spatial modulation (Fig. 1). Conductive nanostructures are created at the $LaAlO_3/SrTiO_3$ interface using a positively biased c-AFM tip placed in contact with the $LaAlO_3$ surface, locally switching the interface to a conducting state because of local protonation of the $LaAlO_3$ surface (*26*, *27*). We perturb the electron waveguide structure by superimposing a periodic transverse modulation to the device (Fig. 1). The path for a sinusoidal waveguide oriented along the x direction is given by $y(x) = y_0 + y_k \sin(kx)$, where y_0, y_k, and k are parameters that can be programmed. The impact of this modulation on the transverse mode, expressed using the basis of unperturbed states ($|m, n, s\rangle$), is expected to be dominated by the $|1,0, s\rangle$ state, with a higher correction from the $|2,0, s\rangle$ state (Fig. 1B).

RESULTS

Four-terminal magnetotransport data for a serpentine superlattice (device A) is shown in Fig. 2. Measurements are taken at or near the base temperature of a dilution refrigerator (T = 25 mK), as a function of out-of-plane magnetic field $|B| \leq 18$ T and chemical potential μ, which is controlled by the voltage on a local side gate. Device design parameters are summarized in Table 1. The four-terminal conductance G as a function of μ and B (Fig. 2A) shows quantized plateaus that result from Landauer quantization, similar to what is observed for unperturbed (straight) electron waveguides.

The "parent" subband structure of these electron waveguides—specifically, the ratio between the lateral and vertical confinement energies—determines how closely spaced the modes are and how well resolved features can be. In the two devices that we focus on here, the vertical confinement energies are approximately 100 μeV (device A) and 250 μeV (device B). The spacing of these energies is believed to be determined by local strain variations from subsurface ferroeleastic domains that freeze in at T = 105 K. As will be discussed below, these variations in waveguide parameters are not correlated with the unique transport features associated with the serpentine modulation. In addition, the devices show a number of fractional conductance plateaus. Two features are highlighted in red and shown in expanded detail in Fig. 2C. The conductance value of this fractional feature evolves down from the $\sim 1e^2/h$ plateau, reaching a value of $\sim 0.4e^2/h$ at B = 18 T. A smaller fractional conductance feature, $\sim 0.2e^2/h$ near-zero magnetic field, remains stable until about B = 1 T, and then decreases in magnitude with increasing B field before disappearing at $B \approx 5$ T. Several fractional conductance states are observable at higher overall conductances, which are also tunable with a magnetic field, e.g., a feature between $1.5e^2/h$ and $1.8e^2/h$. In many instances, G increases beyond the plateau value,

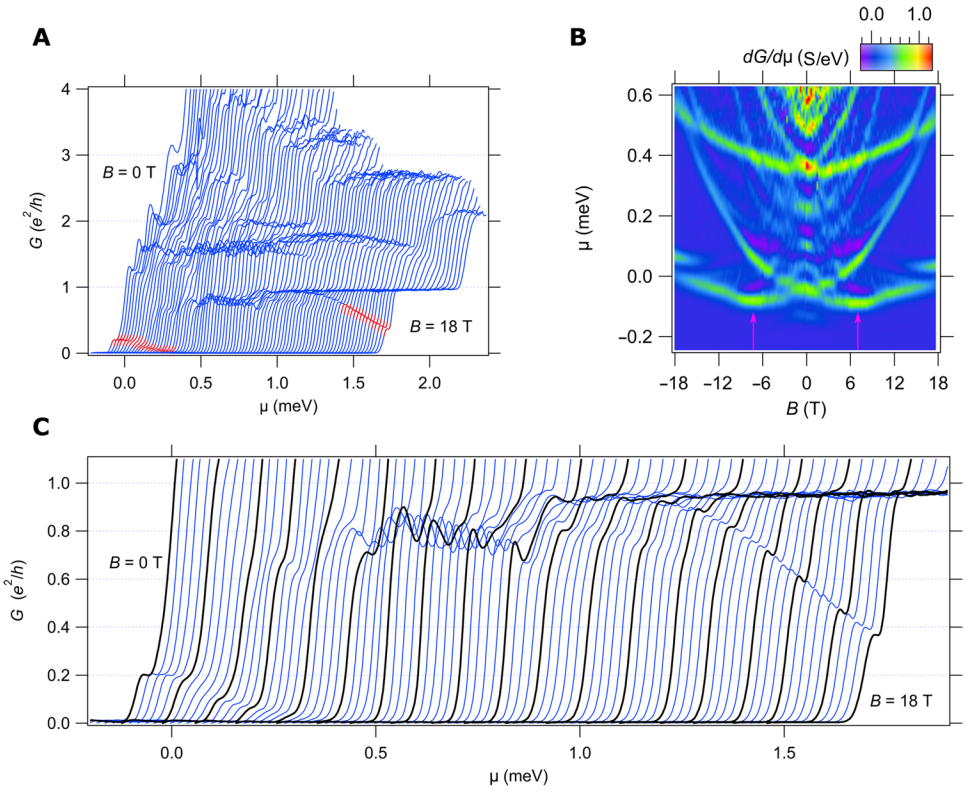

Fig. 2. Magnetotransport for serpentine superlattice device A. (**A**) Conductance, *G*, plotted as a function of chemical potential μ and applied magnetic field *B* from 0 T (leftmost) to 18 T (rightmost). Curves are offset for clarity. Fractional conductance features below the $1e^2/h$ plateau are hightlighted in red. (**B**) Transconductance $dG/d\mu$ as a function of magnetic field *B* and chemical potential μ. Light (red/yellow/green) regions indicate increasing conductance, i.e., when new subbands become available. Dark blue regions indicate zero transconductance or conductance plateaus. Purple regions are regions of negative transconductance and indicate decreasing conductance. The minima of the lowest subband occur at finite *B* field values, highlighted with pink arrows. (**C**) Zoom-in of the fractional conductance features below the $1e^2/h$ plateau. Curves at 1-T intervals are highlighted in black.

Table 1. Writing parameters for serpentine superlattice devices. Devices A and B were written on the same canvas (30 μm by 30 μm area).

Device	Amplitude (nm)	Wavelength (nm)	Periods
A	5	10	40
B	5	11.5	34

before decreasing and stabilizing at the plateau value (this can be seen in parameter regimes for when $dG/d\mu < 0$).

Transconductance maps $dG/d\mu$, when plotted versus *B* and μ (Fig. 2B), provide additional insight into the transport characteristics of these serpentine superlattices. In the color scheme, bright green/yellow/red regions ($dG/d\mu > 0$) represent increases in conductance that generally correspond to introduction of new 1D subbands. Dark blue regions ($dG/d\mu \approx 0$) represent flat conductance plateaus, while purple regions ($dG/d\mu < 0$) correspond to regions of negative transconductance.

One standout feature of the transconductance is a shifting of the lowest subband minima to a nonzero value of the magnetic field ($B = -7.4$ T and $B = 7.1$ T). In this range of magnetic fields, a large overshoot in the conductance is also observed, followed by a region of decreasing conductance. A second feature, observed in two ranges of magnetic field, is the existence of magnetic field–tunable plateaus, seen near-zero magnetic field and in the range 12 to 18 T.

Qualitatively similar behavior is also observed for device B (fig. S1), which is created in a similar manner. Unlike device A, device B shows excess conductance characteristic of superconductivity near-zero magnetic field rather than a fractional conductance plateau (fig. S2). The transconductance map (fig. S1B) also shows some asymmetries in field, which are due to slow temporal drifting of the chemical potential.

The high magnetic field $B = 18$ T fractional conductance feature in device A is examined as a function of temperature *T* and μ (Fig. 3). At the lowest temperature ($T = 25$ mK), the fractional feature appears as a dip in the conductance at around $0.4e^2/h$. The dip flattens out with increasing temperature until it disappears at ~200 mK. The $1e^2/h$ plateau, however, persists up to 750 mK, the highest temperature that was measured. Figure 3B shows the transconductance map $dG/d\mu$ as a function of μ and *T*. All temperatures reported were measured at the mixing chamber stage of the dilution refrigerator.

The conductance and transconductance maps as a function of four-terminal voltage V_{4t} and side gate voltage V_{sg} are shown in Fig. 4 (A and C), respectively. Linecuts of the conductance at zero

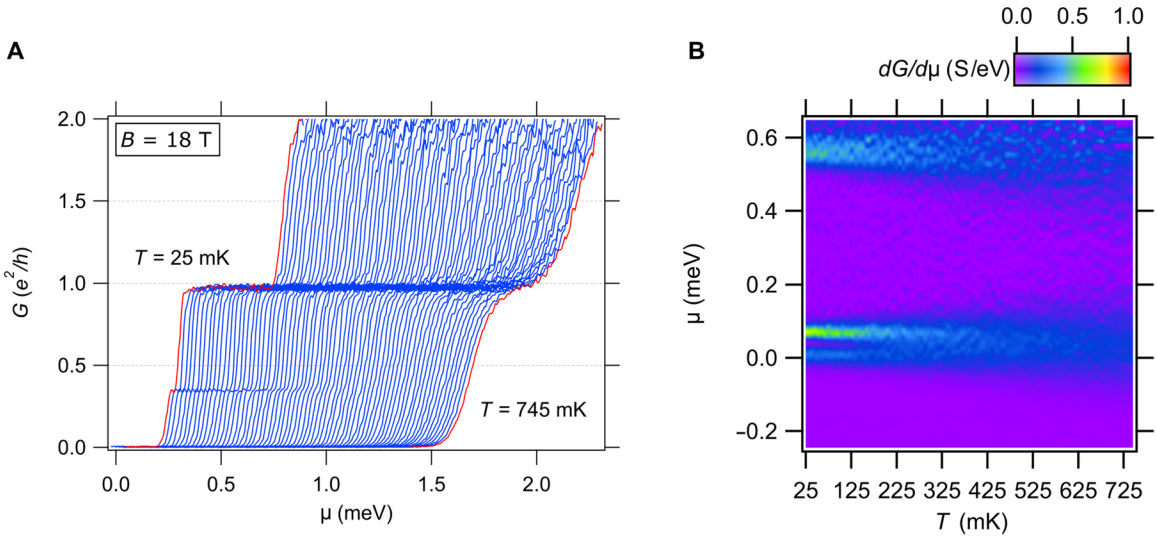

Fig. 3. Temperature dependence of device A. (**A**) Conductance G as a function of chemical potential μ at $B = 18$ T for temperatures from $T = 745$ to 25 mK. Temperatures are measured at the mixing chamber of the dilution refrigerator. (**B**) Transconductance $dG/d\mu$ versus temperature T and chemical potential μ. The fractional conductance feature disappears at around 200 mK, while the $1e^2/h$ conductance plateau is still visible at 745 mK, the highest measured temperature.

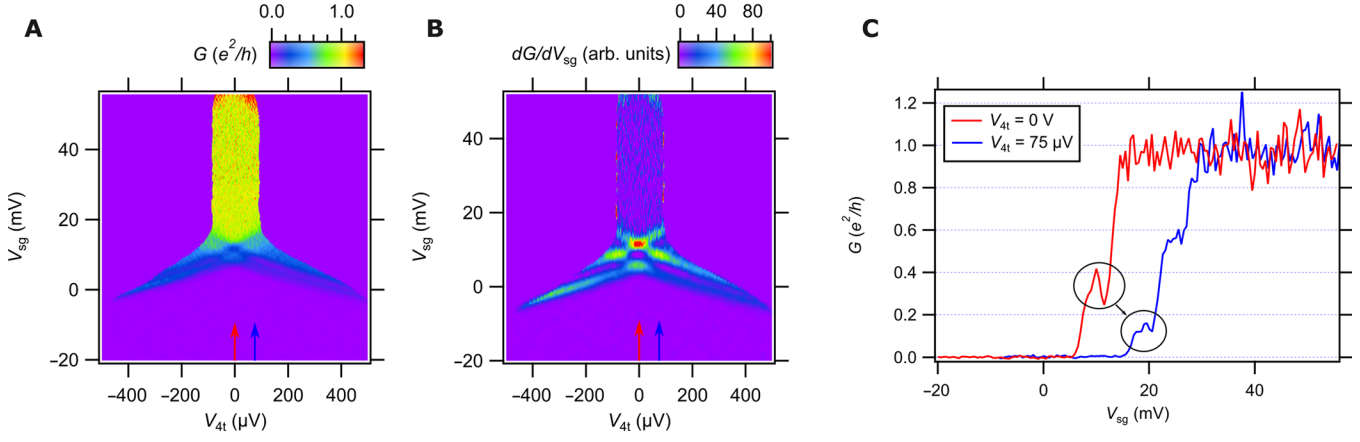

Fig. 4. Finite-bias spectroscopy for device A. (**A**) Conductance map for device A at $B = -18$ T as a function of four-terminal voltage V_{4t} and side gate voltage V_{sg}. Conductance linecuts at $V_{4t} = 0$ V and 75 μV are shown in (**C**). (**B**) Transconductance map corresponding to (A). Red and blue arrows indicate locations of linecuts in (C). The transconductance maps show the diamond feature characteristic of ballistic transport. Conductance linecuts show fractional conductance features below the $1e^2/h$ plateau. At zero bias, the conductance feature appears at ~$0.3e^2/h$ and at finite bias at around half that value ~$0.15e^2/h$. Curves are offset for clarity. All data are taken at $T = 25$ mK.

bias and at a finite bias of $V_{4t} = 75$ μV are shown in Fig. 4 (B and D), respectively. The transconductance map shows a diamond structure characteristic of transport for ballistic systems (*28*, *29*). Large finite biases give rise to half-plateaus due to unevenly populated subbands. The diamond structure implies that the conductance features are not the result of energy-dependent transmission through the device. The value of the feature at zero bias is around $0.3e^2/h$ and is reduced to approximately half that value at finite bias, $0.15e^2/h$.

DISCUSSION

By perturbing the path of a ballistic electron waveguide, we find that it is possible to modify the spin-dependent subband structure in a manner that is consistent with an engineered spin-orbit interaction and results in the creation of new fractional conductance states. The origin of the spin-orbit interactions can be understood in a few different ways. First off, we can discount hypotheses that ascribe these features to "random" effects that are associated, for example, with defects or imperfections. These characteristic features are not observed in control devices where the serpentine modulation is not introduced. The most naive explanation recognizes that the serpentine path of the electrons exposes propagating electrons, with momentum $\vec{k} = k\hat{x}$, to a spatially periodic alternating electric field, $\vec{E}_{\text{eff}}(x) = E_0 \sin(kx)\,\hat{y}$, which, in the moving reference frame of the electrons, corresponds to an alternating effective magnetic field $\vec{B}_{\text{SO}} \propto \vec{k} \times \vec{E}_{\text{eff}}$ that is aligned with the $\hat{z}$ axis. The resulting

spin-orbit field is expected to cause a spin-dependent energy shift of the subband minima by $\pm|\vec{B}_{SO}|$, consistent with our experimental findings (Fig. 2B). We note that periodic reversal of spin-orbit interactions can lead to a phenomenon known as "ballistic spin resonance" (*30*). A more sophisticated approach would take into account the fact that, in the basis of the unperturbed (straight) nanowire, the matrix elements that lead to hybridization with other lateral modes (highlighted in Fig. 1B) are enhanced in the serpentine waveguide, and hence, the magnitude of the Rashba spin-orbit interaction is correspondingly enhanced. Details of such a calculation are beyond the scope of the current manuscript but are nevertheless important for describing numerically accurate models of the engineered spin-orbit interactions.

The second main experimental observation concerns the fractional conductance plateaus that exist both in zero magnetic field and in higher magnetic fields. In some cases, the plateaus are preceded by conductance peaks. Fractional conductance states are typically an indication of strong electron-electron interactions. Well-known examples are the fractional quantum hall effect (*31*) and the "0.7" anomaly, which is commonly observed in quantum point contact devices (*32*) and which is attributed to strong interactions (*33*). There have been theoretical predictions of fractional conductance states in clean 1D systems with arbitrarily many channels and strong (repulsive) electron-electron interactions (*34*, *35*). Oreg *et al.* (*34*) studied 1D wires with spin-orbit coupling and found that in wires with strong interactions and low densities, fractional quantized conductances were predicted. This theory predicts a plateau at $0.2e^2/h$, which usually requires broken time reversal symmetry, which is inconsistent with the observed feature at $0.2e^2/h$ in our system at $B = 0$ T. These fractional states arise due to correlated scattering processes from different channels that can lead to fractional conductance plateaus at various rational fractions. The underlying scattering process relies on two ingredients: (i) multiple channels from which to scatter in the forward and reverse directions and (ii) strong electron-electron interactions that support this correlated exchange of momenta. The Shavit-Oreg theory (*35*) was recently compared to experiments from Kumar *et al.* (*36*), in which fractional conductance plateaus were observed in 1D GaAs-based quantum wires. While both the GaAs-based 1D wire and the $LaAlO_3/SrTiO_3$ nanowires are ballistic, the nature of the electron-electron interactions is fundamentally different for these two materials. That is to say, in GaAs, it is repulsive, while in $LaAlO_3/SrTiO_3$, it is strongly attractive (*19*–*21*, *37*). Many of the devices show signs of superconductivity at $B = 0$ T (fig. S2D), indicating that the interactions in these devices are attractive. The fact that such similar phenomena are identified in both systems is interesting and raises the question: To what extent can the $LaAlO_3/SrTiO_3$ system be modeled as a system with effectively repulsive interactions? It is known theoretically that there is a mapping between the repulsive U and attractive U Hubbard models (*38*). Perhaps, this mapping can be used to understand the attractive side of the phase diagram.

Quasi-1D superlattice devices with engineered properties may provide a building block for more complex quantum systems, for example, topological phases in coupled arrays of quantum wires (*39*–*41*). It may also be possible to observe Majorana fermions in this system (*42*). With the engineering of a spin-orbit interaction, we may have the missing ingredient in $LaAlO_3/SrTiO_3$ nanowire devices. It is also worth emphasizing that these are real electronic materials and not just simulations, with engineerable properties that can be integrated with other materials or incorporated into real electronic devices.

METHODS

$LaAlO_3/SrTiO_3$ samples were grown using pulsed laser deposition described in more detail elsewhere (*43*). Electrical contact was made to the interface by ion milling and depositing Ti/Au electrodes. c-AFM writing was performed by applying a voltage bias between the AFM tip and the interface, with a 1-gigohm resistor in series. Writing was performed in 30 to 40% relative humidity using an Asylum MFP-3D AFM. Written samples were then transferred into a dilution refrigerator. Four-terminal measurements were performed using standard lock-in techniques at a reference frequency of 13 Hz and an applied AC voltage of 100 μV.

SUPPLEMENTARY MATERIALS

Supplementary material for this article is available at http://advances.sciencemag.org/cgi/content/full/6/48/eaba6337/DC1

REFERENCES AND NOTES

1. T. Giamarchi, *Quantum Physics in One Dimension* (Oxford Univ. Press, 2003).
2. R. P. Feynman, Simulating physics with computers. *Int. J. Theor. Phys.* **21**, 467–488 (1982).
3. J. I. Cirac, P. Zoller, Goals and opportunities in quantum simulation. *Nat. Phys.* **8**, 264–266 (2012).
4. I. M. Georgescu, S. Ashhab, F. Nori, Quantum simulation. *Rev. Mod. Phys.* **86**, 153–185 (2014).
5. D. Jaksch, P. Zoller, The cold atom hubbard toolbox. *Annals Phys.* **315**, 52–79 (2005).
6. J. G. Bohnet, B. C. Sawyer, J. W. Britton, M. L. Wall, A. M. Rey, M. Foss-Feig, J. J. Bollinger, Quantum spin dynamics and entanglement generation with hundreds of trapped ions. *Science* **352**, 1297–1301 (2016).
7. J. Zhang, P. W. Hess, A. Kyprianidis, P. Becker, A. Lee, J. Smith, G. Pagano, I.-D. Potirniche, A. C. Potter, A. Vishwanath, N. Y. Yao, C. Monroe, Observation of a discrete time crystal. *Nature* **543**, 217–220 (2017).
8. A. A. Houck, H. E. Türeci, J. Koch, On-chip quantum simulation with superconducting circuits. *Nat. Phys.* **8**, 292–299 (2012).
9. J. Salfi, J. A. Mol, R. Rahman, G. Klimeck, M. Y. Simmons, L. C. L. Hollenberg, S. Rogge, Quantum simulation of the Hubbard model with dopant atoms in silicon. *Nat. Commun.* **7**, 11342 (2016).
10. K. K. Gomes, W. Mar, W. Ko, F. Guinea, H. C. Manoharan, Designer dirac fermions and topological phases in molecular graphene. *Nature* **483**, 306–310 (2012).
11. J. R. Abo-Shaeer, C. Raman, J. M. Vogels, W. Ketterle, Observation of vortex lattices in Bose-Einstein condensates. *Science* **292**, 476–479 (2001).
12. P. Engels, I. Coddington, P. C. Haljan, V. Schweikhard, E. A. Cornell, Observation of long-lived vortex aggregates in rapidly rotating Bose-Einstein condensates. *Phys. Rev. Lett.* **90**, 170405 (2003).
13. Y.-J. Lin, R. L. Compton, K. Jiménez-García, J. V. Porto, I. B. Spielman, Synthetic magnetic fields for ultracold neutral atoms. *Nature* **462**, 628–632 (2009).
14. Y.-J. Lin, K. Jiménez-García, I. B. Spielman, Spin–orbit-coupled Bose–Einstein condensates. *Nature* **471**, 83–86 (2011).
15. A. Hamo, A. Benyamini, I. Shapir, I. Khivrich, J. Waissman, K. Kaasbjerg, Y. Oreg, F. von Oppen, S. Ilani, Electron attraction mediated by Coulomb repulsion. *Nature* **535**, 395–400 (2016).
16. Y.-Y. Pai, A. Tylan-Tyler, P. Irvin, J. Levy, Physics of $SrTiO_3$-based heterostructures and nanostructures: A review. *Rep. Prog. Phys.* **81**, 036503 (2018).
17. C. Cen, S. Thiel, G. Hammerl, C. W. Schneider, K. E. Andersen, C. S. Hellberg, J. Mannhart, J. Levy, Nanoscale control of an interfacial metal–insulator transition at room temperature. *Nat. Mat.* **7**, 298–302 (2008).
18. C. Cen, S. Thiel, J. Mannhart, J. Levy, Oxide nanoelectronics on demand. *Science* **323**, 1026–1030 (2009).
19. A. Annadi, G. Cheng, H. Lee, J.-W. Lee, S. Lu, A. Tylan-Tyler, M. Briggeman, M. Tomczyk, M. Huang, D. Pekker, C.-B. Eom, P. Irvin, J. Levy, Quantized ballistic transport of electrons and electron pairs in $LaAlO_3/SrTiO_3$ nanowires. *Nano Lett.* **18**, 4473–4481 (2018).
20. G. Cheng, M. Tomczyk, S. Lu, J. P. Veazey, M. Huang, P. Irvin, S. Ryu, H. Lee, C.-B. Eom, C. S. Hellberg, J. Levy, Electron pairing without superconductivity. *Nature* **521**, 196–199 (2015).

21. M. Briggeman, M. Tomczyk, B. Tian, H. Lee, J.-W. Lee, Y. He, A. Tylan-Tyler, M. Huang, C.-B. Eom, D. Pekker, R. S. K. Mong, P. Irvin, J. Levy, Pascal conductance series in ballistic one-dimensional $LaAlO_3/SrTIO_3$ channels. *Science* **367**, 769–772 (2020).
22. M. B. Shalom, M. Sachs, D. Rakhmilevitch, A. Palevski, Y. Dagan, Tuning spin-orbit coupling and superconductivity at the $SrTiO_3/LaAlO_3$ interface: A magnetotransport study. *Phys. Rev. Lett.* **104**, 126802 (2010).
23. A. D. Caviglia, M. Gabay, S. Gariglio, N. Reyren, C. Cancellieri, J.-M. Triscone, Tunable Rashba spin-orbit interaction at oxide interfaces. *Phys. Rev. Lett.* **104**, (2010).
24. R. M. Lutchyn, J. D. Sau, S. D. Sarma, Majorana fermions and a topological phase transition in semiconductor-superconductor heterostructures. *Phys. Rev. Lett.* **105**, 077001 (2010).
25. Y. Oreg, G. Refael, F. von Oppen, Helical liquids and majorana bound states in quantum wires. *Phys. Rev. Lett.* **105**, 177002 (2010).
26. F. Bi, D. F. Bogorin, C. Cen, C. W. Bark, J.-W. Park, C.-B. Eom, J. Levy, "Water-cycle" mechanism for writing and erasing nanostructures at the $LaAlO_3/SrTiO_3$ interface. *Appl. Phys. Lett.* **97**, 173110 (2010).
27. K. A. Brown, S. He, D. J. Eichelsdoerfer, M. Huang, I. Levy, H. Lee, S. Ryu, P. Irvin, J. Mendez-Arroyo, C.-B. Eom, C. A. Mirkin, J. Levy, Giant conductivity switching of $LaAlO_3/SrTiO_3$ heterointerfaces governed by surface protonation. *Nat. Commun.* **7**, 10681 (2016).
28. L. I. Glazman, A. V. Khaetskii, Nonlinear quantum conductance of a lateral microconstraint in a heterostructure. *Europhys. Lett. (EPL)* **9**, 263–267 (1989).
29. N. K. Patel, L. Martin-Moreno, M. Pepper, R. Newbury, J. E. F. Frost, D. A. Ritchie, G. A. C. Jones, J. T. M. B. Janssen, J. Singleton, J. A. A. J. Perenboom, Ballistic transport in one dimension: Additional quantisation produced by an electric field. *J. Phys. Condens. Matter* **2**, 7247–7254 (1990).
30. S. M. Frolov, S. Lüscher, W. Yu, Y. Ren, J. A. Folk, W. Wegscheider, Ballistic spin resonance. *Nature* **458**, 868–871 (2009).
31. G. Cheng, A. Annadi, S. Lu, H. Lee, J.-W. Lee, M. Huang, C.-B. Eom, P. Irvin, J. Levy, Shubnikov–de haas–like quantum oscillations in artificial one-dimensional $LaAlO_3/SrTiO_3$ electron channels. *Phys. Rev. Lett.* **120**, 076801 (2018).
32. K. J. Thomas, J. T. Nicholls, M. Y. Simmons, M. Pepper, D. R. Mace, D. A. Ritchie, Possible spin polarization in a one-dimensional electron gas. *Phys. Rev. Lett.* **77**, 135–138 (1996).
33. M. Pepper, J. Bird, The 0.7 feature and interactions in one-dimensional systems. *J. Phys. Condens. Matter* **20**, 160301 (2008).
34. Y. Oreg, E. Sela, A. Stern, Fractional helical liquids in quantum wires. *Phys. Rev. B* **89**, 115402 (2014).
35. G. Shavit, Y. Oreg, Fractional conductance in strongly interacting 1D systems. *Phys. Rev. Lett.* **123**, 036803 (2019).
36. S. Kumar, M. Pepper, S. N. Holmes, H. Montagu, Y. Gul, D. A. Ritchie, I. Farrer, Zero-magnetic field fractional quantum states. *Phys. Rev. Lett.* **122**, 086803 (2019).
37. G. Cheng, M. Tomczyk, A. B. Tacla, H. Lee, S. Lu, J. P. Veazey, M. Huang, P. Irvin, S. Ryu, C.-B. Eom, A. Daley, D. Pekker, J. Levy, Tunable electron-electron interactions in $LaAlO_3/SrTiO_3$ nanostructures. *Phys. Rev. X* **6**, 041042 (2016).
38. A. C. Y. Li, J. Koch, Mapping repulsive to attractive interaction in driven–dissipative quantum systems. *New J. Phys.* **19**, 115010 (2017).
39. C. L. Kane, R. Mukhopadhyay, T. C. Lubensky, Fractional quantum hall effect in an array of quantum wires. *Phys. Rev. Lett.* **88**, 036401 (2002).
40. J. Klinovaja, P. Stano, D. Loss, Topological floquet phases in driven coupled rashba nanowires. *Phys. Rev. Lett.* **116**, 176401 (2016).
41. C. L. Kane, A. Stern, B. I. Halperin, Pairing in Luttinger liquids and quantum hall states. *Phys. Rev. X* **7**, 031009 (2017).
42. V. Mourik, K. Zuo, S. M. Frolov, S. R. Plissard, E. P. A. M. Bakkers, L. P. Kouwenhoven, Signatures of majorana fermions in hybrid superconductor-semiconductor nanowire devices. *Science* **336**, 1003–1007 (2012).
43. G. Cheng, P. F. Siles, F. Bi, C. Cen, D. F. Bogorin, C. W. Bark, C. M. Folkman, J.-W. Park, C.-B. Eom, G. Medeiros-Ribeiro, J. Levy, Sketched oxide single-electron transistor. *Nat. Nanotechnol.* **6**, 343–347 (2011).

Acknowledgments

Funding: J.Levy acknowledges support from a Vannevar Bush Faculty Fellowship, funded by ONR (N00014-15-1-2847), the National Science Foundation (DMR-1609519, PHY-1913034), and the Department of Energy (DE-SC0014417). Work at the University of Wisconsin was supported by funding from the DOE Office of Basic Energy Sciences under award number DE-FG02-06ER46327 (C.-B.E.). **Author contributions:** M.B., P.I., and J.Levy conducted the experiments. J.Li and M.H. processed the samples. H.L., J.-W.L., K.E., and C.-B.E. synthesized the thin films and performed structural and electrical characterizations. All authors reviewed the manuscript. **Competing interests:** The authors declare that they have no competing interests. **Data and materials availability:** All data needed to evaluate the conclusions in the paper are present in the paper and/or the Supplementary Materials. Additional data related to this paper may be requested from the authors.

Submitted 19 December 2019
Accepted 9 October 2020
Published 25 November 2020
10.1126/sciadv.aba6337

Citation: M. Briggeman, J. Li, M. Huang, H. Lee, J.-W. Lee, K. Eom, C.-B. Eom, P. Irvin, J. Levy, Engineered spin-orbit interactions in $LaAlO_3/SrTiO_3$-based 1D serpentine electron waveguides. *Sci. Adv.* **6**, eaba6337 (2020).

ScienceAdvances

Engineered spin-orbit interactions in $LaAlO_3/SrTiO_3$-based 1D serpentine electron waveguides

Megan Briggeman, Jianan Li, Mengchen Huang, Hyungwoo Lee, Jung-Woo Lee, Kitae Eom, Chang-Beom Eom, Patrick Irvin and Jeremy Levy

Sci Adv **6** (48), eaba6337.
DOI: 10.1126/sciadv.aba6337